7 Light-induced Volume Changes in Chalcogenide Glasses

S. Kugler[a,b], J. Hegedüs[a,c], and K. Kohary[d]

[a]*Department of Theoretical Physics, Budapest University of Technology and Economics, H-1521 Budapest, Hungary*
[b]*Department of Electronics and Computer Engineering, Tokyo Polytechnic University, Japan*
[c]*Department of Theoretical Physics and Material Sciences Center, Philipps University Marburg, Renthof 5 D-35032 Marburg, Germany*
[d]*Department of Materials, University of Oxford, Parks Road, Oxford OX1 3PH, UK*
Corresponding author's e-mail: kugler@eik.bme.hu

7.1. INTRODUCTION

Chalcogenide glasses are disordered solids, which contain a considerable amount of chalcogen atoms (S, Se, and Te). In the stable condensed phases chalcogenide elements form covalent bonds with two nearest neighbors in accordance with the $8 - N$ rule. These atoms have six electrons in the outermost shell with a configuration of s^2p^4. Electrons in s states do not participate in bonding since these states have energies well below those of the p states. Two

covalent bonds are formed between chalcogen atoms by two p electrons, but the other elec-
tron pair – also called a lone pair (LP) – remains unbonded.

The structure of pure amorphous selenium (a-Se) – a representative chalcogenide material
– can be described as a random mixture of rings and helical chains accompanied by coor-
dination defects. The trigonal phase consists of infinite helical chains, and the monoclinic
phase's main unit is an eight-membered selenium ring. In these structures the bond length
is close to 2.38 Å, the bond angle 100°, and the dihedral angle 102°, which remain mainly
preserved also in the amorphous phase. Beyond the disorder introduced by the random
arrangement of chains and rings in a-Se the one- and three-fold coordination defects (C1
and C3) also play a decisive role. The average coordination number, however, remains still
close to two. According to the Phillips–Thorpe model a-Se is considered to have an under-
constrained network due to its average coordination number being two. In an amorphous
structure where coordination defects modify the continuous random network the presence
of dangling bonds is expected due to the existing unpaired electrons. However, no electron-
spin resonance (ESR) signal has been observed in a-Se. A possible explanation of this
phenomenon is that the defects are not neutral: one-fold coordinated atoms are negatively
charged (C1) and three-fold coordinated atoms are positively charged (C3), which are called
valence alternation pairs (VAPs).

Chalcogenide glasses exhibit various changes in structural and electronic properties
during bandgap illumination, like photo-induced volume change, photodarkening, and
photo-induced change in the phase state (photo-crystallization and photo-amorphization). A
size effect can be observed: photodarkening cannot be induced in As_2S_3 films which are
thinner than 50 nm [7.1]. These phenomena do not occur in the crystalline chalcogenides
nor in any other amorphous semiconductors. The microscopic structural changes are facil-
itated by two factors common to chalcogenide glasses: the low average coordination number
and the structural freedom of the noncrystalline state. During the illumination some of the
films can expand (a-As_2S_3, a-As_2Se_3, etc.), and some shrink (a-GeS_2, a-$GeSe_2$, etc.) [7.2].
Several investigations have been carried out in order to provide an explanation of these phe-
nomena [7.3–7.8]. It has been established that there is a configurational rearrangement with
changes in atomic coordination in the vicinity of the excitation [7.5–7.7]. In a simplistic
model such changes in the local bonding environment were explained by the formation of
VAPs [7.5]. In amorphous selenium, the model material of chalcogenide glasses, the for-
mation of new inter-chain bonds has also been suggested [7.6]. However, an atomistic study
of amorphous selenium has revealed that the structural rearrangements are less local than
used in such simple models and has given evidence that further possible bond formations
and bond breakings are responsible for photo-induced effects [7.7]. We proposed a simple,
unified description of the photo-induced volume changes in chalcogenides based on tight-
binding (TB) molecular dynamics (MD) simulations of amorphous selenium [7.8]. We have
found that the microscopic rearrangements in the structure (like bond breaking and bond
formation) are responsible for the macroscopic volume change under illumination. The first
in situ surface-height measurement [7.9] on amorphous selenium was carried out recently
and supports our proposed mechanism. Recently, two excellent books appeared on this topic
[7.10, 7.11].

The layout of this chapter is as follows: Section 2 gives an overview on our MD com-
puter code. The details of high-quality, void-free sample preparation using our code can be
found in Section 3. The two subsequent sections contain our microscopic and macroscopic
descriptions of photo-induced volume changes.

E2

7.2 SIMULATION METHOD

We have recently developed a molecular dynamics (MD) computer code (ATOMDEP program package) to simulate the preparation procedures of real amorphous structures (growth by atom-by-atom deposition on a substrate and rapid quenching) [7.12–7.16]. A standard velocity Verlet algorithm was applied in our MD simulations in order to follow the atomic-scale motions. To control the temperature we applied the velocity-rescaling method. We chose $\Delta t = 1$ fs or 2 fs for the time step, depending on the temperature. In our works the growth of amorphous carbon [7.12], silicon [7.13, 7.14], and selenium [7.15, 7.16] films were simulated by this MD method. This computer code is convenient for investigating photo-induced volume changes as well if the built-in atomic interaction can handle the photoexcitation.

For calculating the interatomic forces in a-Se we used tight-binding (TB) [7.16, 7.17] and self-consistent field tight-binding (SCF-TB) [7.16, 7.18] models. TB parameterization [7.17] has been introduced for disordered selenium following the techniques developed by Goodwin et al. [7.19]. It was thoroughly tested by MD calculations in liquid and amorphous phases and the results were compared to experiments and to *ab initio* calculations. The agreement with experiments and *ab initio* calculations is rather good apart from the fact that the number of coordination defects in the solid and liquid phases is higher than the experimentally measured values. The authors have improved their TB Hamiltonian by including the Hubbard correction [7.18]. This implies that either the algorithm has to be made self-consistent or the perturbation theory must be applied. Our choice was the first alternative. For a reasonable accuracy only a few SCF and MD steps were needed. Convergence criteria were considered to be satisfied if the deviation of atomic charges between the actual and the previous iterations was less than 0.01 electron/atom. First, we constructed a tight-binding Hamiltonian, and then diagonalized it. After obtaining a solution, we added the Hubbard terms and recalculated the Hamiltonian matrix. The procedure was repeated until the necessary convergence was reached. The Hamiltonian matrix changed only slightly in one MD step, due to the small atomic movements. Therefore, we could use the eigenvectors from the previous MD step as the starting point in the self-consistency cycle. A convergence problem occurred when we tried to use the SCF method. The solution oscillated, and did not converge at the optimized value of 0.875 eV for the Hubbard parameter. To handle this issue we introduced a damping in the SCF cycles by linearly combining the new solution with the previous one. This method slowed down the convergence speed, but eliminated the oscillations as well.

To test our computer code we performed two test runs [7.20]. Crystalline forms of selenium consist of chains and eight-membered rings. It is very likely that these local arrangements can be found in noncrystalline forms of selenium as well. The initial configuration of the eight-membered ring in our simulation had bond lengths of 2.38 Å and bond angles of 102°. Dihedral angles were 100°. For the eighteen-membered selenium chain (with 1-dimensional periodic boundary condition) these values were: 2.36 Å, 100°, and 98°, respectively. Every Se atom had two first-neighbors, i.e. there was no coordination defect. Before illumination (photoexcitation) the individual ring and the chain were relaxed for 4 ps at $T = 500$ K. During this period the structures were stable. When a photon was absorbed an electron from the highest occupied molecular orbital (HOMO) was transferred to the lowest unoccupied molecular orbital (LUMO). This is a simple model of photoexcitation when an electron is shifted from the valence band to the conduction band (electron–hole

pair creation). After excitation one bond length in the ring started to increase and bond-breaking occurred. A similar result was published [7.21] by a Japanese group for S_8. They performed MD simulation within the framework of density functional theory in the local density approximation. In our second MD simulation we investigated the linear chain structure. The same procedure was performed to model the excitation. A very similar result was obtained; a bond inside the chain was broken immediately after a HOMO electron was excited. Two snapshots of this process can be seen in Figure 7.1.

7.3 SAMPLE PREPARATION

To mimic the thin-film structures, we fabricated glassy networks, for which we applied periodic boundary conditions (PBC) in two dimensions [x,y]. The samples were open in the z direction. When we illuminated the cell, it could expand or shrink into the open direction. The volume changes in the sample can be derived by measuring the distance between atoms at the two open ends. The initial simulation-cell geometry was a rectangular box of size $12.78 \times 12.96 \times 29.69$ (*xyz* in Å). The 162-atom sample had an initial density of $4.33\,\text{g/cm}^3$.

We prepared our samples from the liquid phase by rapid quenching. Our 'cook and quench' sample preparation procedure was as follows: first we set the temperature of the system to 5000 K for the first 300 MD steps. During the following 2200 MD steps, we decreased linearly the temperature from 700 K to 250 K, driving the sample through the glass transition and reaching the condensed phase. Then we set the final temperature to 20 K and relaxed the sample for 500 (1 ps) MD steps. The closed box was opened in the z-direction at the 3000th MD step. We thus obtained two surfaces with an increased number of one-fold coordinated atoms and increased potential energy. This final topology corresponded to a thin-film structure. One problem remained: the localized vibration modes at the surface were excited by the opening procedure. This caused an inhomogeneity in the temperature distribution: the sample had higher temperatures at the ends. Therefore, we homogenously redistributed the atomic kinetic energies according to the Maxwell–Boltzmann distribution, to speed up the thermalization process. We did this three times at the 4000th, 6000th, and 7000th MD steps. The Hubbard parameter, U, was also changed
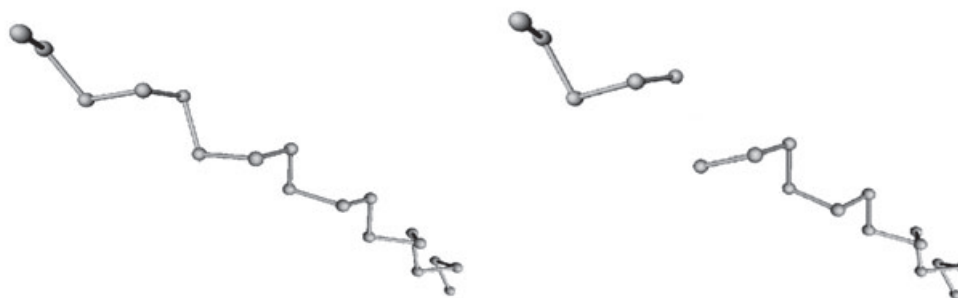

Figure 7.1   Left panel: a snapshot of an 18-atom linear chain at room temperature. Right panel: the same linear chain after excitation

during quenching. By increasing U, one can expect a greater tendency to form a nearly fully two-fold coordinated structure, which is claimed to be the situation for selenium. Therefore, we set the Hubbard parameter at 5 eV during the quenching in the first 4000 MD steps. After the opening procedure was completed, during the relaxation phase at the 4000th MD step we restored U from 5 eV to 0.875 eV, which is the optimized value according to Lomba et al. [7.18]. The system was relaxed for at total of 40 000 MD steps (80 ps) at 20 K.

The most important steps of the preparation procedure can be seen in Figures 7.2–7.5. The initial structure was a bulk glassy selenium network. As in the first phase (0–0.6 ps) the temperature was set at 5000 K in the first MD step, and the potential energy abruptly increased from −540 eV to −480 eV (Figure 7.3). This means that the initial bonding
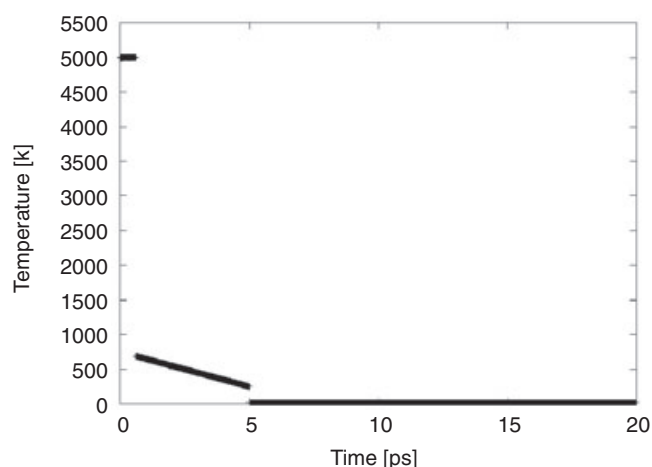

Figure 7.2   Temperature as a function of time during the sample preparation
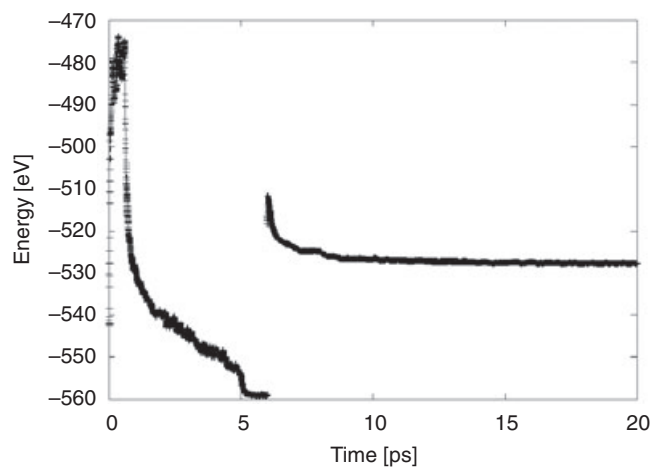

Figure 7.3   A typical curve of the potential energy of the sample vs time during preparation
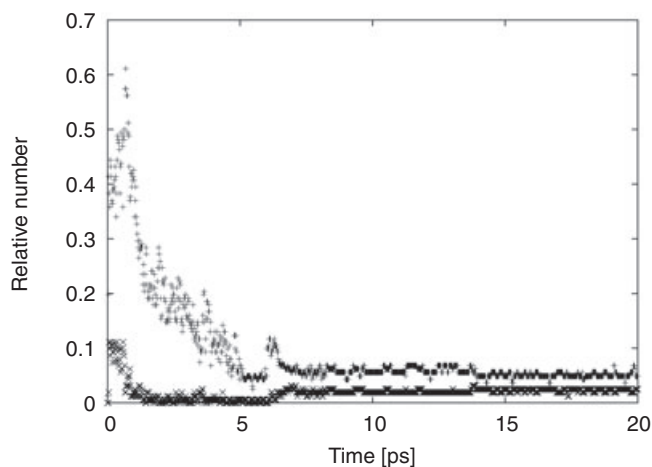
Figure 7.4   Time development of the relative numbers of 3-fold ($\times$) and 1-fold ($+$) coordinated atoms
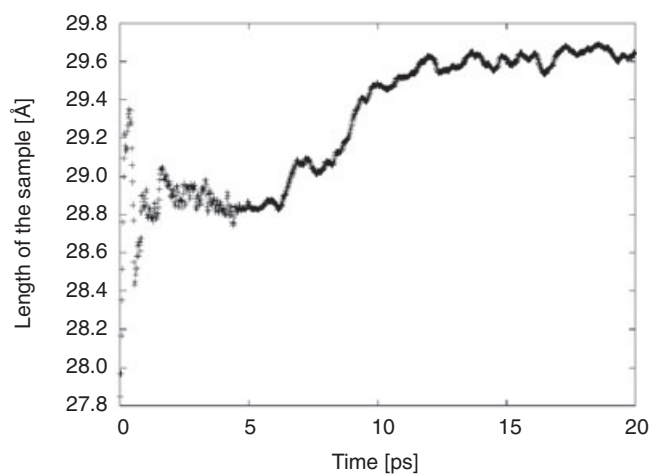

Figure 7.5   Length of the sample during preparation

topology was completely destroyed since at high temperatures all the bonds break immediately. Here, two atoms were considered bonded when the bond length between them was less than 2.7 Å. The relative number of one-fold coordinated atoms was about 40% and that of the three-fold coordinated atoms was 10% during the first 0.6 picoseconds. At 0.6 picoseconds, when the temperature was set to be about 700 K, this situation changed drastically, the percentage of one-fold and three-fold coordinated atoms decreased to 20–25% and 1–2%, respectively. At this point the potential energy decreased by 60 eV within less than 0.1 ps. In the second phase (0.6–5 ps), as we reduced the temperature further down from 700 K to 250 K the number of one-fold coordinated atoms decreased from 20% to 5% but the number of three-fold coordinated atoms did not change (See Figure 7.4).
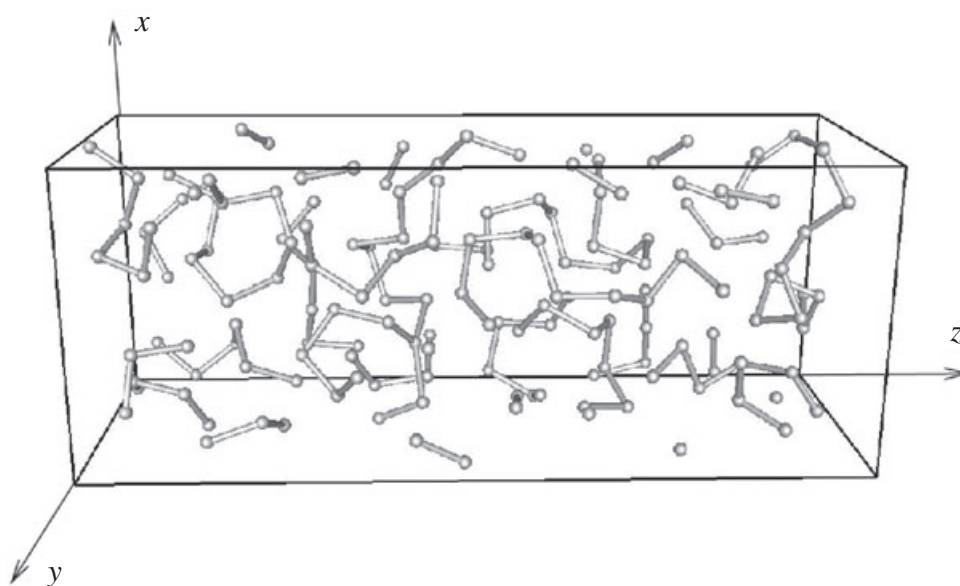
E2

Figure 7.6   Snapshot of a final glassy selenium network. The sample can expand in the z direction, since at the ends we do not apply periodic boundary conditions

The cooling rate during this phase was about 10^{14} K/s. At 5 ps, another sudden decrease by 5 eV in the potential energy (Figure 7.3) was observed when the temperature was reduced from 250 K to 20 K. After this the system was equilibrated for another 1 ps and then the network was opened by releasing the PBC in the z-direction. Examining the potential energy (Figure 7.3), an immediate increase from -560 eV to -510 eV can be seen. This corresponds to breaking approximately 10–20 bonds at the surface. Subsequently, a quick recovery occurred, involving about a 5–10 eV decrease in the potential energy in 0.5 picoseconds and then another 5–10 eV decrease on a longer time scale (10–100 picoseconds). The first corresponds to the formation of new bonds, as one sees in the change of coordination numbers (Figure 7.4), while the second corresponds to a large-scale structural change, i.e. volume expansion (Figure 7.5). During the last five picoseconds the sample became stable and the volume no longer changed significantly. If we changed the initial velocities of the atoms only during the first MD step we fabricated topologically different glassy networks under similar physical conditions. For a 162-atom system, one SCF step on a 1200 MHz computer took about 2–3 seconds. The visualization of the structures and of the time development of the system was carried out by self-written Java software, JGLMOL, which is available free of charge [7.22].

Samples prepared at 20 K had densities from 3.95 to 4.19 g/cm^3. The number of coordination defects ranged from 3 to 12%. Most of these defects were located on the surfaces. The structure consisted mainly of branching chains, but some rings could also be found. The samples were accepted if the volume fluctuation was less than 0.5% in 60 picoseconds. We prepared altogether 30 samples, and 17 were considered to be stable and useful for further studies. One of them is displayed in Figure 7.6. A radial distribution function of a representative sample can be seen in Fig 7.7.
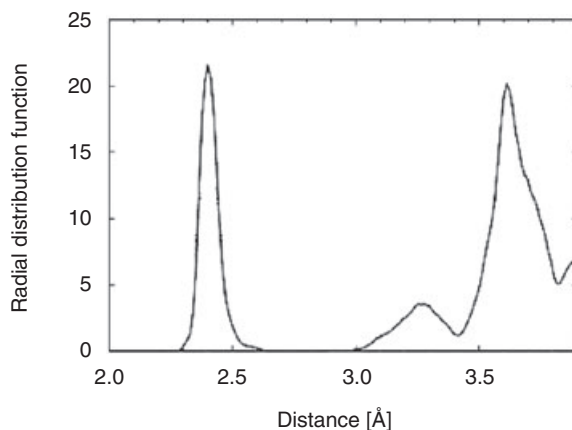
E2

Figure 7.7   Radial distribution function of an amorphous selenium network as a function of atomic distances. The model was prepared by MD simulation at 20 K

7.4 LIGHT-INDUCED PHENOMENA

In amorphous selenium immediately after the absorption of a photon, an electron–hole pair became separated in space [7.8]. Therefore, they can be treated independently, i.e. we can investigate the roles of excited electrons and holes separately. We ran two sets of computer simulations: first, to model the excited electron creation we put an extra electron into the LUMO; and secondly, we annihilated an electron in HOMO (hole creation).

7.4.1 Electron excitation

A covalent bond between two-fold and three-fold coordinated atoms was broken (C2 + C3 $\Rightarrow$ C1 + C2) in the majority of cases when an additional electron was put into the LUMO, as seen in Figure 7.8.

   The bond-breaking significantly affects the bond lengths, alternations between shrinkage and elongation in the vicinity of the broken bond being displayed in Figure 7.8. Our localization analysis revealed that the LUMO was localized at this site before the bond-breaking as it can be seen in Figure 7.9. A release of excitation restores all bond lengths to their original value.

   The time development of photo-induced bond-breaking due to an added electron and the corresponding volume expansion in one of our amorphous selenium sample is shown in Figure 7.10. We have selected one sample (Figure 7.10) from our simulations, which seems to be a typical run. Similar changes were observed in each amorphous selenium network. Before the excitation at 5 ps the bond length was about 2.55 Å. In this particular case bond-breaking occurred at a weaker bond due to the C3 site, which had a larger interatomic separation than the majority of the nearest-neighbor bonds of 2.4 Å. During the illumination, this weaker bond (2.55 Å) increased by 10–20% (in this example to 3 Å) and it decreases to its original value after the de-excitation. (Arrows show the excitation and de-excitations in Figure 7.10.) The volume change follows the bond-breaking and it shows damped oscillations on the picosecond time scale.
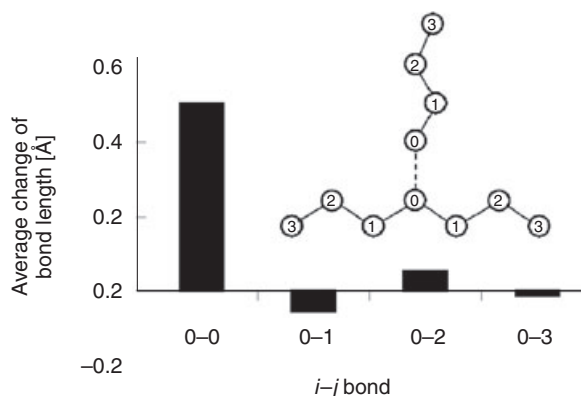
Figure 7.8 Bond breaking and bond-length changes due to electron addition in the LUMO of an amorphous selenium network. Here i and j refer to the numbered atoms in the Figure. The dark rectangles represent the average changes in bond lengths between i–j atoms
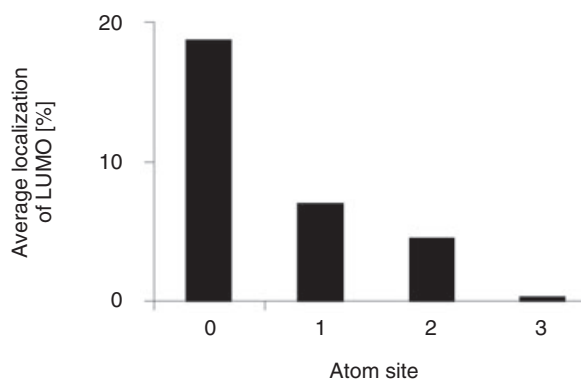
Figure 7.9 Average localizations of LUMO at the atoms 0, 1, 2, 3. See Figure 7.8 for notations

7.4.2 Hole creation

We observed that inter-chain bonds were formed after creation of a hole and they cause contraction of the sample (Figure 7.11). This contraction always appears near to atoms where the HOMO is localized. Since the HOMO is usually localized in the vicinity of a one-fold coordinated atom, the inter-chain bond formation often takes place between a one-fold coordinated atom and a two-fold coordinated atom ($C\{1,0\} + C\{2,0\} \Rightarrow C\{1,1\} + C\{2,1\}$, where the second number means the number of inter-chain bonds). However, sometimes we also observed the formation of inter-chain bonds between two two-fold C2 coordinated atoms ($C\{2,0\} + C\{2,0\} \Rightarrow C\{2,1\} + C\{2,1\}$).

In order to model the collective effect of photo-induced changes in amorphous selenium, we also performed simulations with five excited electron creations and five hole creations. We put five excited electrons from the five highest occupied energy levels (one electron from one level) to the five lowest unoccupied energy levels (again, one electron to each
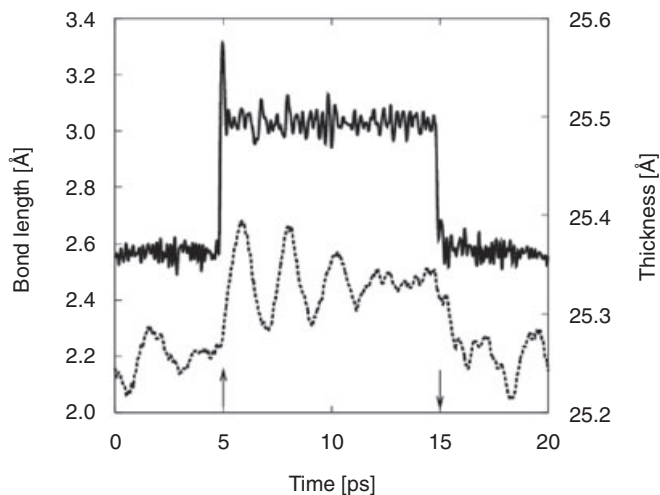
E2

Figure 7.10   Bond length of broken bond (solid line) and thickness of sample (dotted line) during photoexcitation plotted as a function of time. Excitation starts at 5 ps and ends at 15 ps (arrows) (reproduced from J. Hegedüs, K. Kohary, D.G. Pettifor, K. Shimakawa, and S. Kugler, *Phys. Rev. Lett.*, **95**, 206803 (2005). Copyright (2005) by the American Physical Society)
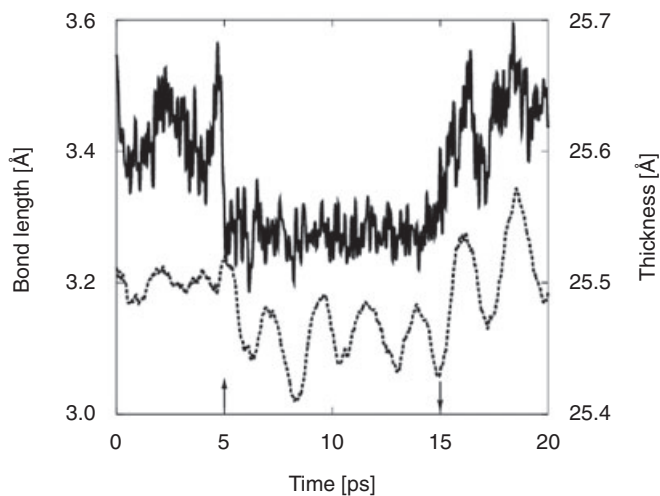

Figure 7.11   Photo-induced local contraction due to the addition of a hole in a-Se as a function of time. Distance between two atoms in different Se chains at sites where HOMO is localized (solid line). Thickness of sample is denoted with dashed line. Hole is created at 5 ps and annihilated at 15 ps (reproduced from J. Hegedüs, K. Kohary, D.G. Pettifor, K. Shimakawa, and S. Kugler, *Phys. Rev. Lett*., **95**, 206803 (2005). Copyright (2005) by the American Physical Society)

level). We found similar effects as described above for single electron/hole creation: bond-breakings and inter-chain bond formations have similar characteristics. Nevertheless, in the five-excited-electron creation case, further bond-breaking occurred not only at the C3 sites, but as well at some C2 sites. In the case of the five-hole creation, we observed that inter-chain bonds were formed between C1 and C2 sites and also between C2 and C2 sites.

The bond-breaking and inter-chain bond formation can be understood in terms of a change in the bond strength before and during the excitations. We calculated the bond energies [7.8, 7.23] within the TB representation. We obtained a decrease in the bonding energy of 0.24 eV after a bond-breaking for a typical case. In contrast, a hole addition leads to an increase in the inter-chain bond energy of 0.042 eV.

7.5 MACROSCOPIC MODELS

7.5.1 Ideal, reversible case [7.8] (a-Se)

The light-induced volume expansion and volume shrinkage in amorphous selenium occur simultaneously and these are additive quantities as our molecular dynamics simulations have confirmed. The expansion of the thickness d_e is proportional to the number of excited electrons n_e ($d_e = \beta_e \, n_e$), while the shrinkage d_h is proportional to the number of created holes n_h ($d_h = \beta_h n_h$), where the parameters β_e and β_h are the average thickness changes caused by an excited electron and a hole, respectively. The time-dependent equation of thickness change can then be written as:

$$\Delta(t) = d_e(t) - d_h(t) = \beta_e n_e(t) - \beta_h n_h(t) \tag{7.1}$$

Assuming $n_e(t) = n_h(t) = n(t)$ we get

$$\Delta(t) = (\beta_e - \beta_h)n(t) = \beta n(t) \tag{7.2}$$

where β is a characteristic constant of different chalcogenide glasses related to photo-induced volume (thickness) change. The sign of this parameter governs whether the material shrinks or expands. The number of electrons excited and holes created is proportional to the duration time of illumination. Their generation rate G depends on the number of incoming photons and on the photon absorption coefficient. After the photon absorption, the separated excited electrons and holes migrate within the amorphous sample and then eventually recombine. A phenomenological equation for this dominant process can be written as:

$$dn_e(t)/dt = G - Cn_e(t)n_h(t) \tag{7.3}$$

where C is a constant. Using $n_e(t) = n_h(t) = n(t)$ and $\Delta(t) = \beta n(t)$, we obtain a fundamental equation for the time-dependent volume change, namely,

$$\mathrm{d}\Delta(t)\big/\mathrm{d}t = G - (C/\beta)\Delta^2(t) \tag{7.4}$$

Solution of this nonlinear differential equation is obtained as:

$$\Delta(t) = \beta(G/C)^{1/2}\tanh\big[(GC)^{1/2}\,t\big] \tag{7.5}$$

Recently, the photo-induced expansion of amorphous selenium films was measured *in situ* for the first time using optoelectronic interference and enhanced by image processing [7.9]. Figure 7.12 shows the measured time evolution of the surface height over the interval of 0–300 s together with its best fit.

 After the light is turned off ($G = 0$), Equation (7.4) can be written as:

$$\mathrm{d}\Delta(t)\big/\mathrm{d}t = -(C/\beta)\Delta^2(t) \tag{7.6}$$

with the solution

$$\Delta(t) = a\big/[a(C/\beta)t + 1] \tag{7.7}$$

Figure 7.13 displays the measured volume change and the fitted theoretical curve to the measured data. Light was switched off at $t = 800$ s.

7.5.2 Nonideal, irreversible case [7.24] (a-As$_2$Se$_3$)

In the ideal case we assumed that each local structure variation was reversible and the original local structure was reconstructed after the electron–hole recombination. However, the
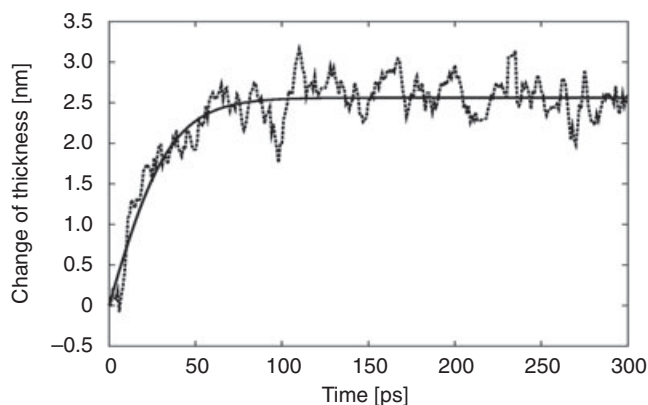

Figure 7.12 Time development of volume expansion in amorphous selenium (dashed line) and its theoretical best fit (solid line)
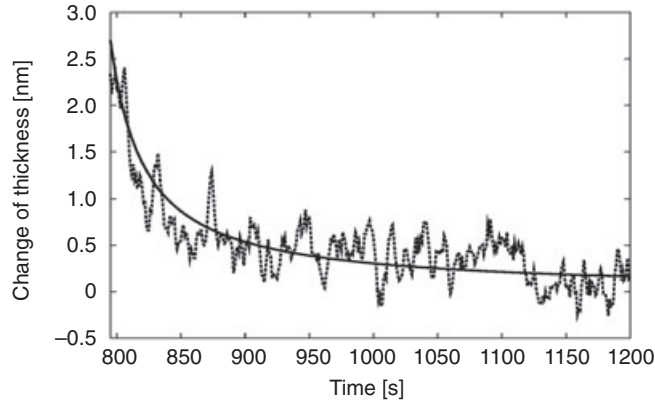
Figure 7.13   The measured shrinkage of a-Se (dashed line) and the fitted curve (solid line) after stopping the illumination

result of a measured volume change on flatly deposited a-As$_2$Se$_3$ film is quite different from the ideal selenium case (see Figure 2b in Ref. [7.9]). To explain the difference we must take into account a large number of irreversible changes in the local atomic arrangement, i.e. after turning off the light the local configuration remains the same and there is no electron–hole recombination. The total volume change includes both the reversible and irreversible changes and it can be written as:

$$\Delta_{\text{total}}(t) = \Delta_{\text{rev}}(t) + \Delta_{\text{irr}}(t) \tag{7.8}$$

The reversible part follows Equations (7.4) and (7.6) during and after the illumination, respectively, with the corresponding solutions given in Equations (7.5) and (7.7).

We now consider the irreversible component. During the illumination, the generation rate of irreversible microscopic change is time dependent. Let's consider that an upper limit exists for the maximum number of electrons and holes causing irreversible changes and let these denoted by $n_{\text{e,irr,max}}$ and $n_{\text{h,irr,max}}$, respectively. To simplify the derivation let us assume that $n_{\text{e,irr,max}} = n_{\text{h,irr,max}}$. In this case, one can write the electron generation rate as:

$$G_{\text{e}}(t) = C_{\text{e}}[n_{\text{e,irr,max}} - n_e(t)] \tag{7.9}$$

Note that there is no recombination term in Equation (7.9). Following Equation (7.4), we obtain that the irreversible expansion is governed by:

$$d\Delta_{\text{irr}}(t)/dt = G_{\text{irr}} - C_{\text{irr}}\Delta(t) \tag{7.10}$$

Equation (7.10) then leads to the solution:

$$\Delta_{\text{irr}}(t) = (G_{\text{irr}}/C_{\text{irr}})(1 - \exp\{-C_{\text{irr}}t\}) \tag{7.11}$$

E2

Using Equation (7.11) in Equation (7.8), the best fit of the volume expansion [$\Delta_{\text{total}}(t)$], and that of the reversible and irreversible parts [$\Delta_{\text{rev}}(t)$, and $\Delta_{\text{irr}}(t)$] are displayed in Figure 7.14.

After illumination there is no volume change caused by the irreversible microscopic effects. Figure 7.15 shows the shrinkage after switching off the illumination, which is the fit as obtained in the reversible case.
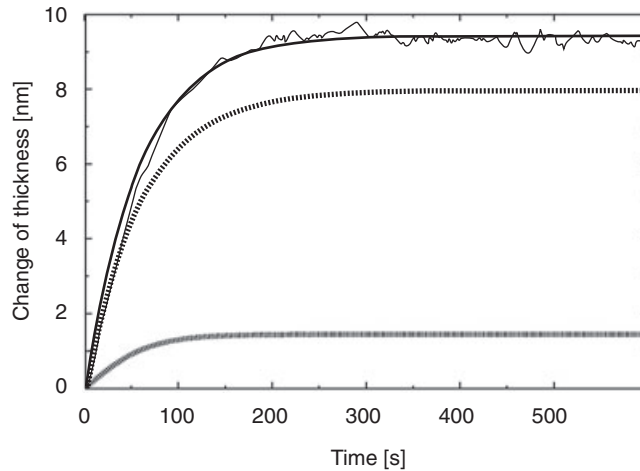

Figure 7.14   Time development of volume expansion of a-As$_2$Se$_3$. Thin solid line is the measured curve, thick solid line is the fitted line [$\Delta_{\text{total}}(t) = \Delta_{\text{rev}}(t) + \Delta_{\text{irr}}(t)$]. Lower dashed curve is the best fit of $\Delta_{\text{rev}}(t)$, while the upper one is that of the irreversible part $\Delta_{\text{irr}}(t)$
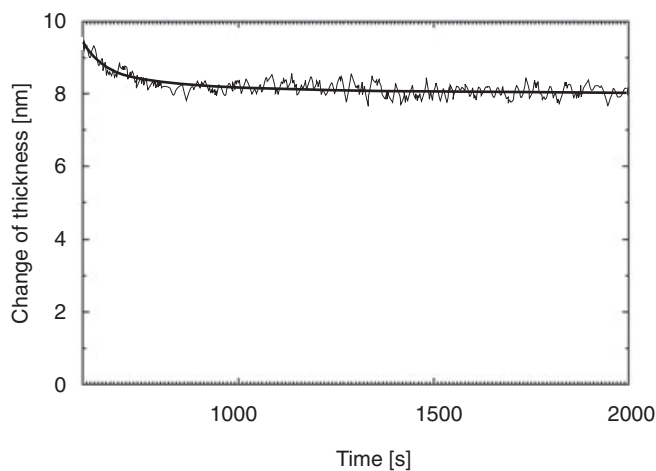

Figure 7.15   The measured decay (thin solid line) and the fitted theoretical curves (thick solid line) for the shrinkage as a function of time after stopping the illumination

7.6 CONCLUSIONS

We have proposed a new explanation for the photo-induced volume changes in chalcogenide glasses. We have found that the covalent bond-breaking occurs in these glasses with excited electrons, whereas holes contribute to the formation of inter-chain bonds. In the ideal situation both processes are reversible. The interplay between photo-induced bond-breaking and inter-chain bond formation leads to either volume expansion or shrinkage. In the nonideal case, only a part of the processes is irreversible and the total expansion includes the reversible and irreversible changes. Our microscopic explanation of the macroscopic photo-induced volume change is consistent with the first *in situ* surface-height measurements.

ACKNOWLEDGEMENT

REFERENCES

[7.1] K. Tanaka, N. Kyoya, and A. Odajima, *Thin Solid Films*, **111**, 195 (1984).

[7.2] Y. Kuzukawa, A. Ganjoo, and K. Shimakawa, *J. Non-Cryst. Solids*, **227–230**, 715 (1998); *Philos. Mag. B*, **79**, 249 (1999).

[7.3] K. Shimakawa, A. Kolobov, and S.R. Elliott, *Adv. Phys*., **44**, 475 (1995).

[7.4] K. Shimakawa, N. Yoshida. A. Gahjoo, A. Kuzukawa, and J. Singh, *Philos. Mag. Lett*., **77**, 153 (1998).

[7.5] H. Fritzsche, *Solid-State Commun*., **99,** 153 (1996).

[7.6] A.V. Kolobov, H. Oyanagi, K. Tanaka, and K. Tanaka, *Phys. Rev. B*, **55**, 726 (1997).

[7.7] X. Zhang and D.A. Drabold, *Phys. Rev. Lett*., **83**, 5042 (1999).

[7.8] J. Hegedüs, K. Kohary, D.G. Pettifor, K. Shimakawa, and S. Kugler, *Phys. Rev. Lett*., **95**, 206803 (2005).

[7.9] Y. Ikeda and K. Shimakawa, *J. Non-Cryst. Solids*, **338**, 539 (2004).

[7.10] J. Singh and K. Shimakawa, *Advances in Amorphous Semiconductors* (Taylor and Francis, London and New York, 2003).

[7.11] *Photo-Induced Metastability in Amorphous Semiconductors*, Edited by A.V. Kolobov (Wiley-VCH, 2003).

[7.12] K. Kohary and S. Kugler, *Phys. Rev. B*, **63**, 193404 (2001).

[7.13] S. Kugler, K. Kohary , K. Kádas, and L. Pusztai, *Solid-State Commun*., **127**, 305 (2003).

[7.14] K. Kohary and S. Kugler, *Mol. Simul*., **30**, 17 (2004).

[7.15] J. Hegedüs, K. Kohary, and S. Kugler, *J. Non-Cryst. Solids*, **338**, 283 (2004).

[7.16] J. Hegedüs and S. Kugler, *J. Phys.: Condens. Matter,* **17,** 6459 (2005).

[7.17] D. Molina and E. Lomba, *Phys. Rev. B*, **60**, 6372 (1999).

[7.18] E. Lomba, D. Molina, and M. Alvarez, *Phys. Rev. B*, **61**, 9314 (2000).

[7.19] L. Goodwin, A.J. Skinner, and D.G. Pettifor, *Europhys. Lett*., **9**, 701 (1989).

E2

[7.20] J. Hegedüs, K. Kohary, S. Kugler, and K. Shimakawa, *J. Non-Cryst. Solids*, **338**, 557 (2004).
[7.21] F. Shimojo, K. Hoshino, and Y. Zempo, *J. Phys.: Condens. Matter*, **10**, L177 (1998).
[7.22] http://www.physik.uni-marburg.de/~joco/JGLMOL.html
[7.23] D. Pettifor, *Bonding and Structure of Molecules and Solids* (Clarendon Press, Oxford, 1995).
[7.24] J. Hegedüs, K. Kohary, and S. Kugler, *J. Non-Cryst. Solids*, in press.

1

QUERY FORM

Dear:

    During the preparation of your manuscript for publication, the questions listed below have arisen. Please attend to these matters and return this form with your proof.

Many thanks for your assistance.

Query References	Query	Remarks
1	AU: Are more details available?	